

IMPACT OF GRAVITY ON THIN-LAYER CELL ELECTROCHEMICAL DEPOSITION*

E. MOCSKOS[†] AND G. MARSHALL[†]

Abstract. Electrochemical deposition (ECD) in thin cells with different orientations relative to gravity leads to complex stable and unstable physicochemical hydrodynamic flows. Here we study the impact of gravity on these flows through a theoretical macroscopic 3D model and its numerical simulation. The model describes the diffusive, migratory, and convective motion of ions in a fluid subject to an electric field through the Nernst-Planck, Poisson, and Navier-Stokes equations, respectively. The equations are written in terms of dimensionless quantities, in particular, the gravity Grashof number, revealing the importance of gravitoconvection. The nonlinear system of partial differential equations is solved on a uniform grid using finite differences and a strongly implicit iterative scheme. In ECD in a cell in a horizontal position, our model predicts the evolution of two gravity-driven convective rolls and concentration shells attached to each electrode. We predict their birth, growth, expansion towards one another, collision, and merger into a single roll that invades the whole cell. In ECD in a cell in a vertical position, cathode above anode, our model predicts that gravity-induced rolls and concentration shells remain locally attached to fingers that grow downwards; thus, global invasion of the cell by gravity-induced rolls is suppressed, leading to a stable stratified flow. In ECD in a cell in a vertical position, cathode below anode, our model predicts the detachment of rolls and concentration shells from each electrode in the form of plumes that expand towards one another, mix, invade the whole cell, and lead to an unstable stratified flow. For ECD, whether in horizontal or vertical position, in the presence of growth, our model predicts the existence of an electrically driven vortex ring at the dendrite tip that interacts with concentration shells and rolls, leading to complex helicoidal flows. Such structures are experimentally observed, suggesting that ion transport underlying dendrite growth is remarkably well captured by our model.

Key words. electrochemical deposition, computational modeling, finite differences, stable physicochemical hydrodynamic flows, unstable physicochemical hydrodynamic flows

AMS subject classifications. 76W05, 76U05, 65Z05, 65C20, 68U20, 65M06, 76D05

1. Introduction. In an electrochemical deposition (ECD) experiment, the electrolytic cell consists of two glass plates sandwiching two parallel electrodes and a metal salt electrolyte. A voltage difference applied between the electrodes produces a ramified deposit by reduction of the metal ions. Depending on the cell geometry, cell orientation relative to gravity, electrolyte concentration, cell voltage, and other parameters, the deposit can be fractal, densely branched or dendritic, or even chaotic. ECD has become a paradigmatic model for the study of growth pattern formation (GPF), that is, the unstable growth of interfaces [1, 3–19, 21, 23–27, 32].

Beyond the dendrite growth, complex physicochemical hydrodynamical ion transport processes take place. Ion transport is mainly governed by diffusion, migration, and convection. Convection is mostly driven by Coulombic forces due to local electric charges and by buoyancy forces due to concentration gradients that lead to density gradients. The relevance of convection, relative to migration and diffusion, for cells with thickness larger than $50\mu\text{m}$ has been demonstrated by a number of researchers [3, 4, 10–12, 14, 15, 18, 21]. In cells with thickness less than $50\mu\text{m}$, diffusion and migration are the dominant modes of ion transport [19].

Convection adds to the complexity of ECD flows, and therefore it is natural to try to reduce it to a negligible level. One possibility is to reduce buoyancy forces by orienting the cell in a vertical position relative to gravity [18]. With this technique, when the cathode (and low-density fluid) is above the anode (and high-density fluid), the invasion of the cell by the

*Received July 24, 2008. Accepted November 12, 2008. Published online on May 22, 2009. Recommended by José Castillo.

[†]Laboratorio de Sistemas Complejos, Departamento de Computación, Facultad de Ciencias Exactas y Naturales, Universidad de Buenos Aires, C1428EGA, Buenos Aires, Argentina (emocksos@dc.uba.ar, marshalg@mail.retina.ar).

gravity-induced rolls is globally suppressed while electroconvection remains. Stratification remains stable as long as there is no growth of dendrites. But as soon as a dendrite appears, stratification breaks down, because the fluid concentration surrounding a downward-growing dendrite tip diminishes, creating a horizontal concentration gradient and thus, locally, gravitoconvection. Away from dendrites, stratification remains stable [18]. However, if the anode (and high-density fluid) is above the cathode (and low-density fluid), an unstable stratification leads to a global convective flow [18].

Figures 1.1–1.7 illustrate the previous discussion. Figure 1.1 shows the experimental setup for ECD in horizontally and vertically oriented cells relative to gravity, respectively.

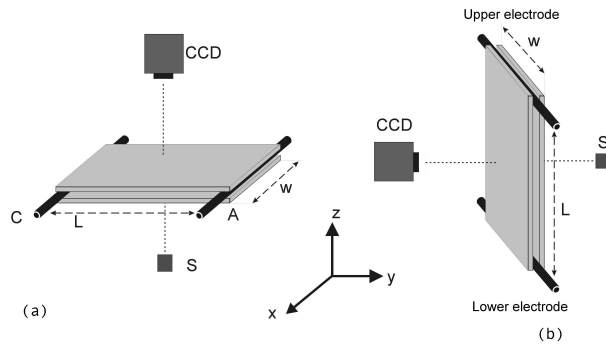


FIG. 1.1. (a) Cell in a horizontal position relative to gravity and (b) cell in vertical position relative to gravity.

Figure 1.2 shows, in a cell in the horizontal position (the plane of the growth is normal to gravity), schlieren images of dendrites growing from the cathode towards the anode (dark pixels) and concentration fronts (bright pixels). A characteristic of ECD growth in horizontal cells is the appearance of a hierarchy of branch sizes rather than a uniform front.

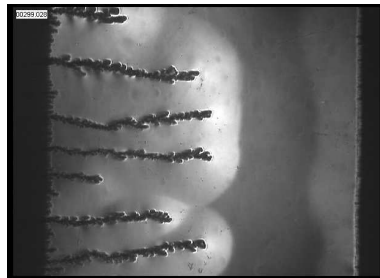


FIG. 1.2. Schlieren image of ECD in a cell in the horizontal position (the plane of the growth is normal to gravity). Copper sulfate solution concentration is 0.5 M, the cell width is 0.2 mm, and the applied constant voltage is 15V (reproduced from [7]).

The concentration variations observed in Figure 1.2 lead to density variations and therefore to the development of gravity-driven convection rolls at the electrodes [18]. This is illustrated in Figure 1.3, which shows a side view of the cell with a roll near the cathode. Moreover, due to local instabilities, a dendrite growth at the cathode is triggered, and local electric charges, and thus Coulombic forces, concentrate at the dendrite tips according to a model developed in [13] (cf. also references cited therein). Each porous filament allows fluid to penetrate its tip and to be ejected from the sides, forming a vortex pair in the plane of the growth driven by the electric force. Figure 1.4 shows a top view of the cell with a pair of counter-rotating vortices, as described in [13].

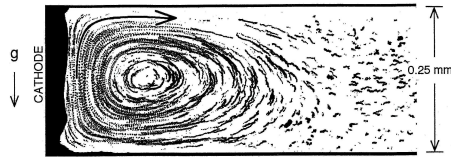


FIG. 1.3. Side view of the cathodic roll visualized with tracer particles (reproduced from [18]).

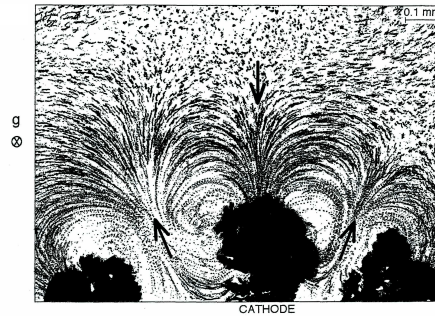


FIG. 1.4. Top view of the vortex ring visualized with tracer particles (reproduced from [18]).

Figure 1.5 shows a schlieren snapshot of the evolution of the deposit front (dark pixels) and the cathodic and anodic concentration fronts (light pixels) in an ECD in a vertical cell with the cathode above the anode. A characteristic of this growth is that the deposit front looks rather uniform on average, and consists of dendrite tips surrounded by tenuous concentration arches that join neighboring tips. The shape of the arches is the result of electroconvection and gravitoconvection.

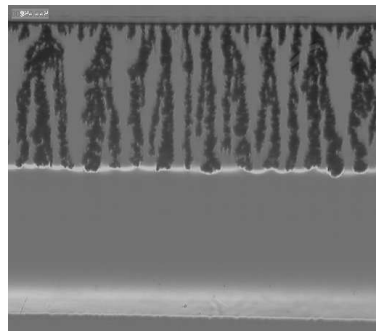


FIG. 1.5. Schlieren image of ECD in a vertically oriented cell (cathode above anode) at 460s giving rise to a globally stable flow. Copper sulfate solution concentration is 0.1M, the cell dimensions are $70 \times 10 \times 0.2 \text{ mm}^3$, and the applied constant current is 5mA.

Figure 1.6 shows an ECD experiment in a vertical cell, cathode above anode, with a small protruding spike (to mimic the behavior of one of the dendrite tips) on an otherwise flat electrode, and the flow surrounding it. Convection is visualized with 200 snapshots of micron-sized tracer particles, spanning an interval of 20 seconds, superposed to show their motion. The tracer particles reveal a pair of counter-rotating vortices, the result of the vector composition of local buoyancy and local electric forces. In this locally unstable regime, local convection prevails, but globally the ECD process is controlled by migration and diffusion and is thus stably stratified.



FIG. 1.6. Visualization of $1\mu\text{m}$ -sized particle trajectories near a spike in the cathode in an ECD in a vertical cell (cathode above anode) giving rise to a locally unstable flow. To show the motion of tracer particles, 200 digital images were superimposed: from 40 to 60s. Copper sulfate solution concentration is 0.1M with 30% glycerol in weight, the cell dimensions are $70 \times 10 \times 0.127\text{ mm}^3$, the applied constant current is 2 mA , and the spike dimensions are $1 \times 0.5 \times 0.127\text{ mm}^3$.

Figure 1.7 shows an experimental schlieren concentration snapshot of an ECD experiment in a vertical cell, anode above cathode. Here, the unstable flow emerges from the development of high-density plumes detaching from the anode and descending, and low-density plumes detaching from the cathode, rising towards the anode, and mixing with plumes coming down. This global gravitoconvection strongly inhibits dendrite growth.

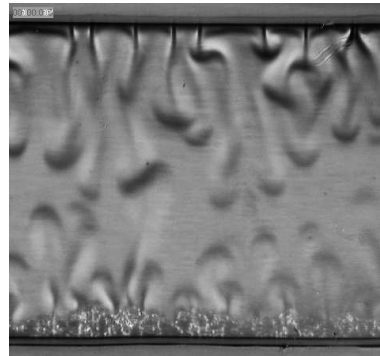


FIG. 1.7. Unstable flow pattern: schlieren image of a vertically oriented cell at 100s. Copper sulfate solution concentration is 0.1M , the cell dimensions are $70 \times 10 \times 0.2\text{ mm}^3$, and the applied constant current is 5 mA .

- To summarize the experimental evidence shown:
- (a) A cell in a horizontal position relative to gravity leads always to a constrained unstable flow regime.
 - (b) A cell in a vertical position with the cathode above the anode comprises two flow regimes:
 - (i) in the absence of dendrites, a globally stable stratified flow regime in which there is no convection and the ECD process is controlled by migration and diffusion;
 - (ii) in the presence of dendrites, a quasi-stable flow regime in a zone near the dendrites, in which there is local convection and the ECD process is controlled by migration, diffusion, and convection; outside that region, the flow is stably stratified.
 - (c) A cell in a vertical position with the anode above the cathode comprises one flow regime: a globally unstable stratified flow, whether with or without dendrites.

A comparison between horizontal and vertical ECD experiments reveals that in the horizontal case, ECD always leads to a constrained unstable flow regime. However, the orientation of the cell walls relative to gravity impedes the development of a full unstable flow as in the case of a vertical cell with the anode above the cathode. Moreover, a characteristic of ECD growth in horizontal cells is the appearance of a hierarchy of branch sizes, while a uniform front appears in the cell in the vertical position when the cathode is above the anode. Since the only change in both cases is the direction of the electric field relative to gravity, no doubt,

gravity is the main cause of these differences in the growth and flow regimes.

The aim of this paper is to study the effect of gravity on ECD through numerical simulations that could lead to new insights of ECD behavior. The paper is organized as follows. Section 2 presents the mathematical and computational models, Section 3 presents the numerical results, and finally Section 4 presents a discussion and draws some general conclusions.

2. Mathematical and computational models. Ion transport in a thin-layer ECD can be described with a mathematical model based on first principles [2, 20, 28, 31], including the Nernst-Planck equations for ion transport, the Poisson equation for the electric potential, and the Navier-Stokes equations for the fluid flow. The 3D dimensionless system of equations can be written as

$$(2.1) \quad \frac{\partial C_i}{\partial t} = -\nabla \cdot \mathbf{j}_i,$$

$$(2.2) \quad \mathbf{j}_i = -M_i C_i \nabla \phi - \frac{1}{Pe_i} \nabla C_i + C_i \mathbf{v},$$

$$(2.3) \quad \nabla^2 \phi = Po \sum_i z_i C_i,$$

$$(2.4) \quad \frac{\partial \boldsymbol{\zeta}}{\partial t} + \nabla \times (\boldsymbol{\zeta} \times \mathbf{v}) = \frac{1}{Re} \nabla^2 \boldsymbol{\zeta} + \sum_i \left[G_{e_i} z_i (\nabla \phi \times \nabla C_i) - G_{g_i} (\nabla \times C_i) \frac{\mathbf{g}}{g} \right],$$

$$(2.5) \quad \boldsymbol{\zeta} = -\nabla^2 \Psi,$$

$$(2.6) \quad \mathbf{v} = \nabla \times \Psi.$$

Here C_i and \mathbf{j}_i are the dimensionless concentration and flux of an ionic species i (for a ternary electrolyte such as $\text{ZnSO}_4/\text{H}_2\text{SO}_4$, $i = \text{C}$ and A , standing for zinc and sulphate); \mathbf{v} , ϕ , $\boldsymbol{\zeta}$, and Ψ are the dimensionless fluid velocity, electrostatic potential, vorticity vector, and velocity potential vector, respectively; and \mathbf{g}/g is a unit vector pointing in the direction of gravity. The quantities $M_i = \mu_i \Phi_0 / x_0 u_0$, $Pe_i = x_0 u_0 / D_i$, $Po = x_0^2 C_0 e / \epsilon \Phi_0$, $Re = x_0 u_0 / \nu$, $G_{e_i} = e C_i \Phi_0 / \rho_0 u_0^2$, and $G_{g_i} = x_0 C_i g \alpha_i / u_0^2$ are the dimensionless migration, Peclet, electric Poisson, Reynolds, electric Grashof, and gravity Grashof numbers, respectively. The quantities z_i , μ_i , and D_i are, respectively, the number of charges per ion, the mobility constant, and the diffusion constant of an ionic species i ; μ_i and z_i are signed quantities, being positive for cations and negative for anions; g is the dimensional gravitational acceleration; e is the electronic charge, ϵ is the permittivity of the medium, and ν is the kinematic viscosity. x_0 , u_0 , ϕ_0 , C_0 , and ρ_0 are reference values of the length, velocity, electrostatic potential, concentration, and fluid density, respectively. For system closure, a Boussinesq-like approximation has been used for the fluid density: $\rho = \rho_0 (1 + \sum_i \alpha_i \Delta C_i)$, where $\alpha_i = \frac{1}{\rho_0} \frac{\partial \rho}{\partial C_i}$.

The system (2.1)–(2.6), with appropriate initial and boundary conditions, is valid in a space-time domain defined by $\mathbf{G} = \Omega(t) \times (0, t)$, where Ω is a three-dimensional region with boundary $\Gamma(t)$; this boundary moves with speed proportional to the norm of the flux \mathbf{j}_i . The boundary conditions for the velocity potential vector are discussed, for instance, by Mallinson and de Vahl Davis [22]: in a plane impermeable surface, the vector is normal to the surface and its gradient is zero; at nonslip surfaces, the tangential derivative of the velocity components is zero.

The computational model solves the previous 3D system of equations, for each time step, in a fixed or variable domain, in a 3D uniform lattice, using finite difference and deterministic

relaxation techniques. The solution is obtained via the system of difference equations:

$$(2.7) \quad \mathbf{W}_k^{n+1} = \sum_j \mathbf{a}_j \mathbf{W}_j^n,$$

where j represents the nearest-neighbor site for the site k ; the summation ranges over all nearest-neighbor sites; \mathbf{W}_k is a vector-valued function whose components are the concentrations A and C , the electrostatic potential ϕ , the vorticity vector ζ , and velocity potential vector Ψ ; and \mathbf{a}_j is a diagonal matrix whose elements contain the nonlinear coefficients of the discretized equations. The resulting solution \mathbf{W}_k^{n+1} is then used to advance the interface with a dielectrical breakdown model (DBM) [30]. The interface is moved at random, proportionate to the flux of cations, i.e.,

$$(2.8) \quad p_k = \frac{|\mathbf{j}_{ck}|}{\sum_i |\mathbf{j}_{ci}|},$$

where k is a nearest-neighbor site to the interface, p_k is the probability of selecting the nearest-neighbor site k to advance the interface, the summation is over all nearest-neighbor sites i to the interface, and \mathbf{j}_{ck} is the flux of cations flowing from the neighbor site k into the aggregation.

In all the simulations presented below a fixed domain is used, and the following set of dimensionless quantities remain constant: $M_A = 1/30$, $M_C = 1/45$, $Pe_A = 600$, $Pe_C = 750$, $Po = 2.3 \times 10^3$, $Ge = 1 \times 10^5$, $Gg_A = 1.5 \times 10^4$, $Gg_C = 1 \times 10^4$, and $Re = 0.1$. Figures are constructed with the graphics software package OpenDX [29].

3. Numerical results. In the following, we present numerical simulations of ECD experiments with the cell in the horizontal position and in the vertical position, cathode above and below anode, respectively. Figure 3.1 shows a sequence of snapshots of ECD with the cell in horizontal position in the presence of three spikes on an otherwise flat electrode. The plots show particle trajectories released at different locations in the cell and anion concentration isosurfaces or concentration shells. The cell is represented using a grid of $80 \times 200 \times 50$ nodes. Particle trajectories serve to track the evolution of the cathodic and anodic convective rolls. They reveal how density currents generate gravity-driven rolls consisting of horizontal cylinders squeezed at their extremes due to lateral wall effects. While the anodic roll remains undisturbed, the cathodic roll is wrapped around the electrode spikes. The snapshots show the precise moment in which the cathodic and anodic rolls collide and merging starts. There is a coalescence among individual rolls of adjacent filament tips, resulting in a more uniform cathodic front. This front is defined by dendrites and their vortex rings, which push the front forward. Trajectories of particles released near the dendrite tips reveal the entangled nature of flow: near the dendrite tips, the fluid is entrained by vortex rings whose basins of attraction are the dendrite tips. However, some particles manage to escape and are entrained by the vortex roll, finally orbiting with a helicoidal motion. Particle trajectories also unveil vortex interactions among themselves in the presence of dendrites, in an analogy with the physical experiments from Figure 1.2.

Figure 3.2 shows snapshots of ECD with the cell in horizontal position, in the presence of three spikes in an otherwise flat electrode. The plots show a vertical cross-section of vortex tube and anion concentration shells. The simulations reveal the evolution of concentration shells which follow closely the evolution of rolls. One of the snapshots shows the precise moment in which the cathodic and anodic concentration fronts collide and slip one over the other. Again, these simulations have some resemblance to the physical experiments of Figures 1.2, 1.3, and 1.4.

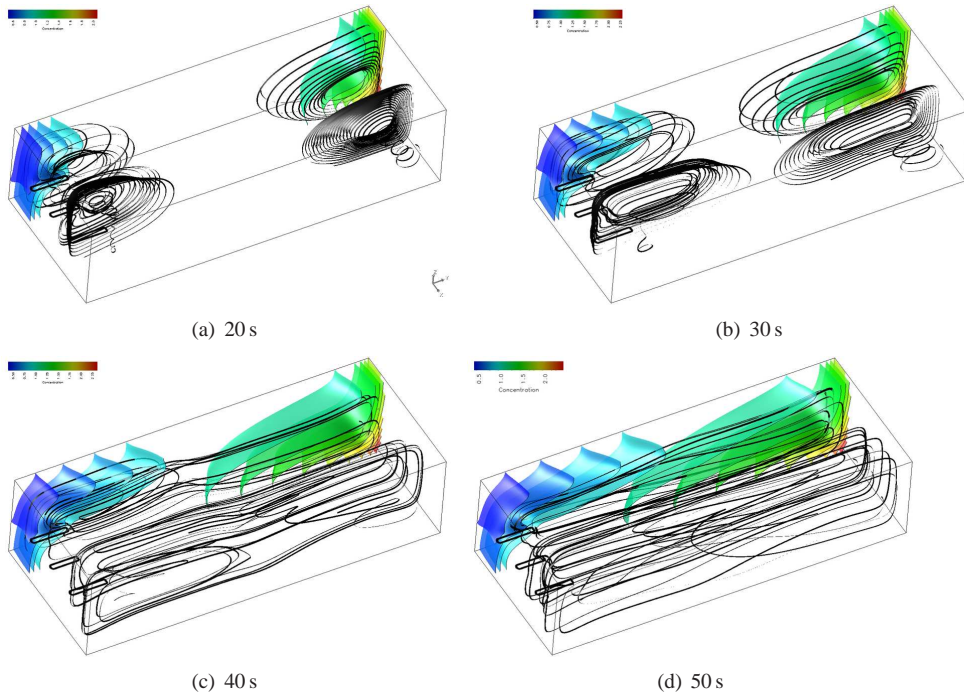


FIG. 3.1. Snapshots of the horizontal cell flow pattern simulation with three spikes at different times: particle trajectories and anion concentration isosurfaces.

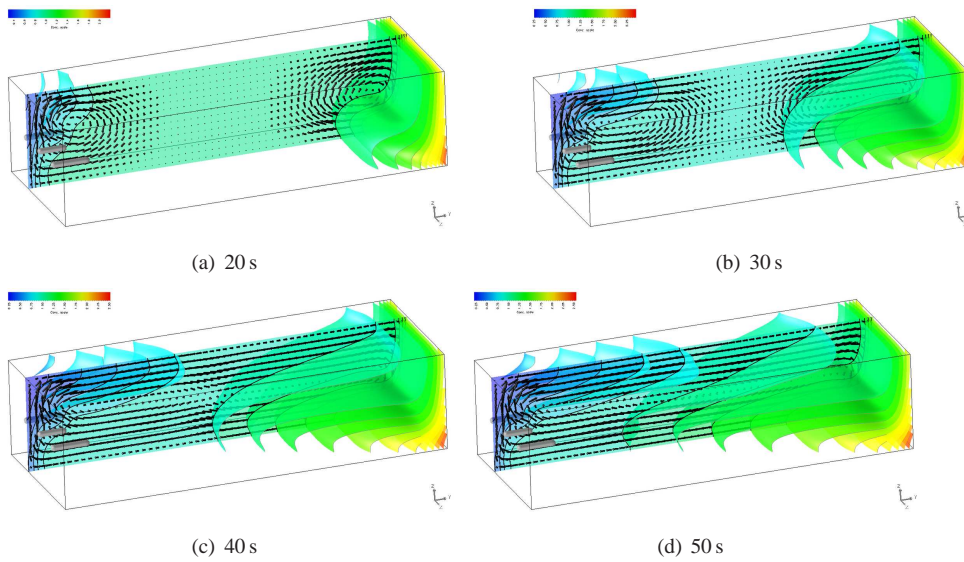
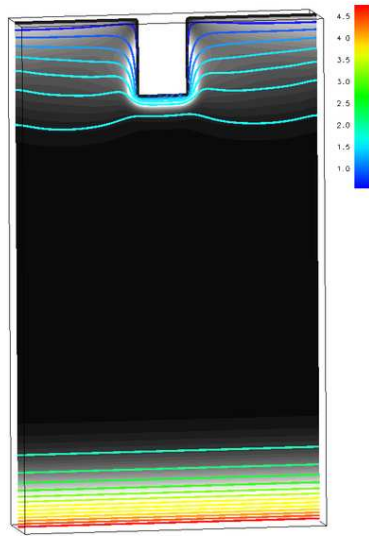


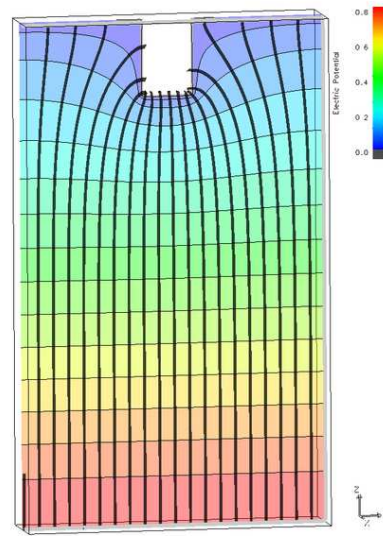
FIG. 3.2. Snapshots of flow pattern simulation near three spikes at different times: velocity field superimposed with anion concentration isosurfaces (clipped to improve visualization).

In the following, we present numerical simulations in a vertical cell (cathode above anode). The cell is represented by a cubic grid of $30 \times 120 \times 200$ nodes.

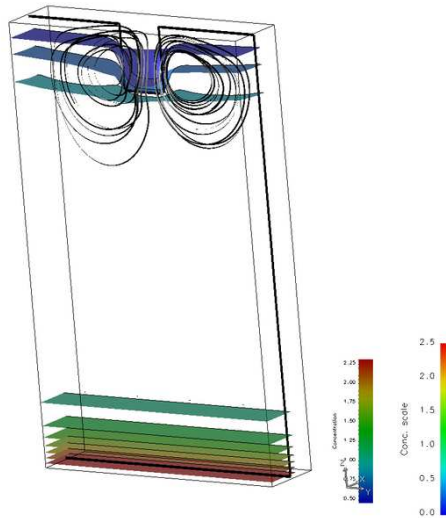
Figure 3.3 shows snapshots of ECD with the cell in a vertical position, cathode above anode, in the presence of one single spike (enlarged) in an otherwise flat electrode.



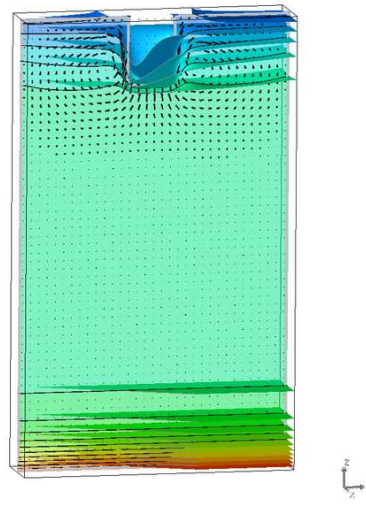
(a) Numerical schlieren image with concentration contour lines superimposed.



(b) Electric field lines superimposed with electrostatic potential contour lines.



(c) Particle trajectories superimposed with anion concentration contour lines.



(d) Velocity field superimposed with anion concentration contour lines.

FIG. 3.3. Flow pattern simulation near a spike in a vertical cell (cathode above anode).

Figure 3.3(a) displays numerical schlieren superimposed on concentration contours. Near the spike, the white zone indicates the vortex tube and ring wrapped around the spike. Figure 3.3(b) displays a geometric form with the approximate shape of a spherical drop (gray area turned slightly transparent) representing an isosurface of the modulus of the electric field, and a cross-section (at spike level) of the electric field lines. The approximate spherical shape of the drop is due to the value of the modulus of the electric field (thresholded); the field strength is constant in a large portion of the cell and only increases near the finger tips. The electric field lines converging to the filament tip are clearly seen in the figure. The drop

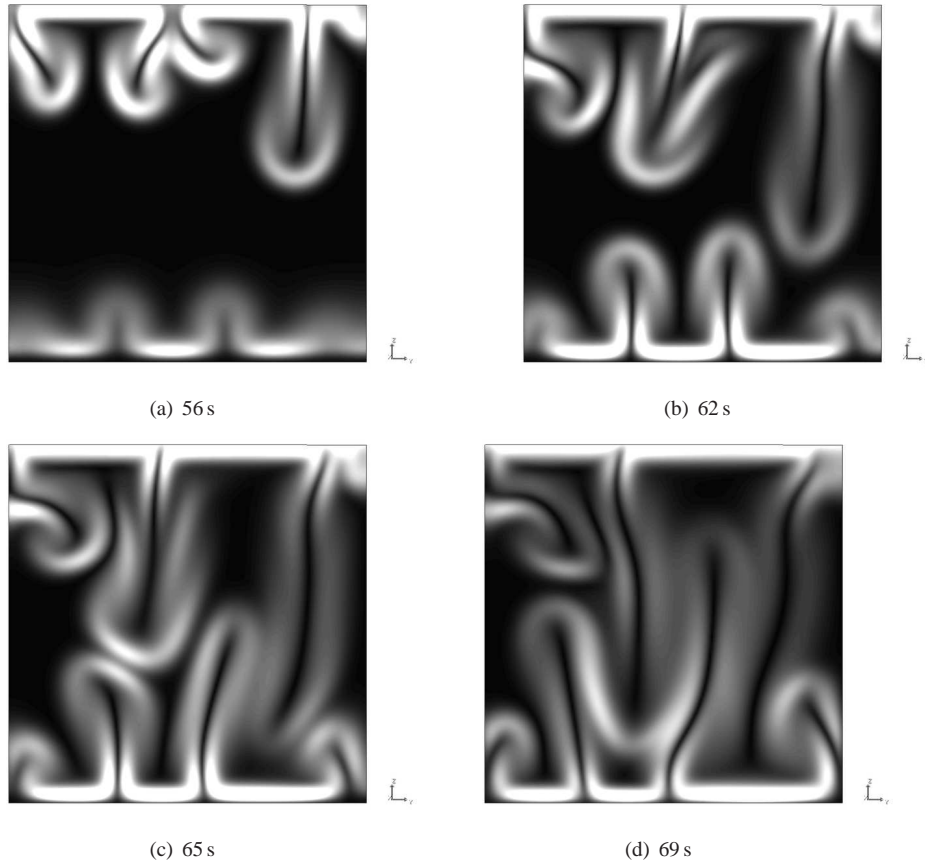


FIG. 3.4. Simulated unstable stratified flow in a vertical cell (cathode below anode): numerical schlieren images of ion concentration.

approximately indicates the space zone inside which there is absence of electroneutrality. In fact, the exact computational zone where electroneutrality is absent can be obtained by the surface of the function defined by the difference between the cation and anion concentration ($\sum_i z_i C_i$). This surface is approximately represented by the drop; we call it the electric spherical drop. Figure 3.3(c) shows concentration shells and particles released near the spike, which give evidence of the superimposed vortex tube and ring. Figure 3.3(d) displays concentration shells and the velocity field. These simulations have some resemblance to the physical experiments of Figures 1.5 and 1.6.

In the following, we present numerical simulations of ECD in a cell in a vertical position, cathode below anode. In this case, the cell is represented by a grid of $20 \times 200 \times 200$ nodes. Figures 3.4 and 3.5 present the simulation of an unstable stratified flow in which dendrites are represented just by one small spike at the cathode center. This configuration is intended to mimic the situation depicted in Figure 1.7. Figure 3.4 shows snapshots of schlieren concentration plumes evolving towards an unstable stratified flow. In these remarkable images, it is clear how high-density concentration plumes detach themselves from the anode at the top, descend, and mix with ascending low-density concentration plumes detaching from the cathode at the bottom. Figure 3.4(d) reveals a fully developed unstable flow. Finally, Figure 3.5 shows detailed images of concentration shells and particle trajectories, their detachment from each electrode, and their encounter and mixing.

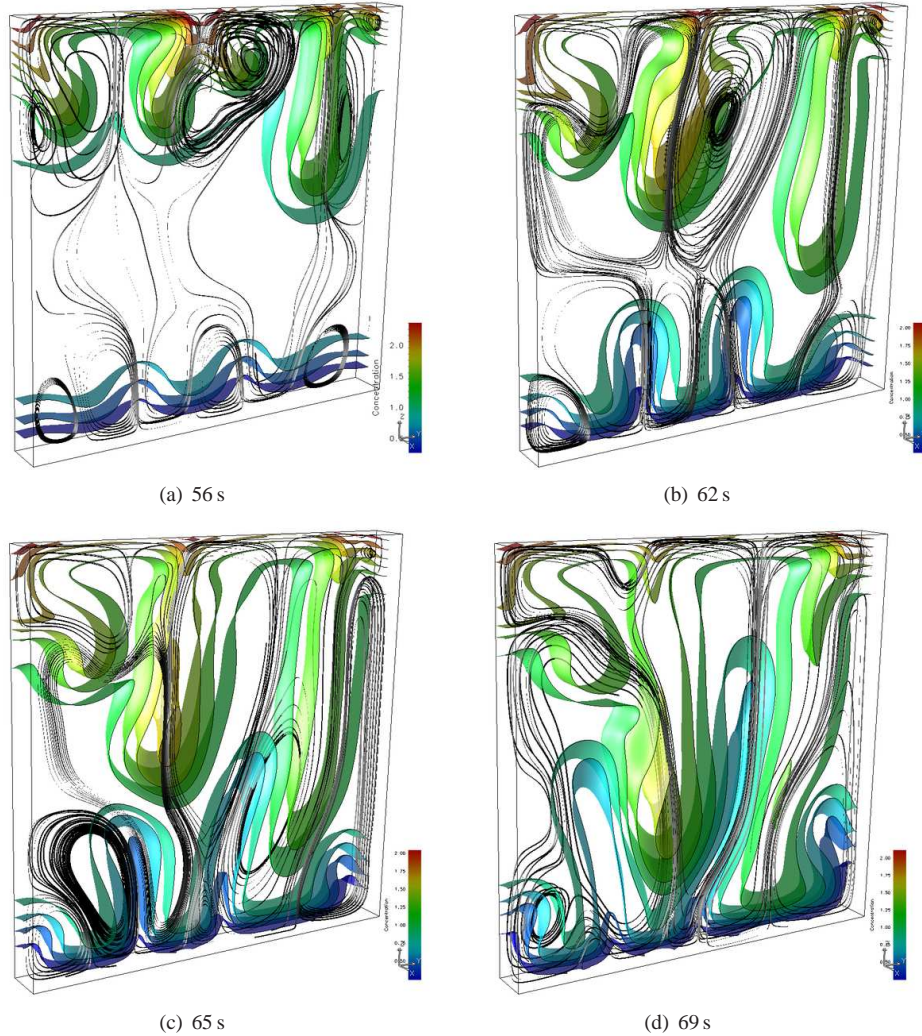


FIG. 3.5. Simulated unstable stratified flow: clipped isosurface of concentration shells and particle trajectories.

4. Discussion. We presented a 3D mathematical macroscopic model for ECD in cells in horizontal and vertical positions relative to gravity, and numerical simulations of that model. The mathematical model and numerical simulations, the latter validated with 2D experimental measurements, allowed the construction of the following more complete predictive phenomenological 3D model.

In a horizontal cell, our model predicts the existence of concentration shells and convection rolls near each electrode, not detaching from them but expanding towards one another, and their interaction with ramified deposits. At the dendrite, the shells and rolls bend and surround the tip, forming a sort of three-dimensional envelope tube which is squeezed by the dendrite tip and which closely follows the evolution of the deposit front.

In a vertical cell, cathode above anode, in the presence of growth, our model predicts that the fluid concentration near a downward-growing tip is lowered, thus generating a vortex tube (driven by gravitoconvection) wrapping the dendrite tip (much as in the case of the horizontal cell in which the dendrite tip is surrounded by rolls). The region close to the anode

is not affected by the growth and remains without convection, giving rise to a global stable stratified flow.

In a vertical cell, cathode below anode, our model predicts an unstable stratified flow in which the cathodic and anodic vortex tubes transform themselves into plumes or tongues expanding towards one another and merging. As a consequence of this mixing, concentration gradients are strongly attenuated.

In horizontal as well as in vertical cells, our model predicts the existence of vortex rings driven by electroconvection and electric spherical drops at the tips of the dendrites, allowing fluid to penetrate at the tip and to be ejected from its sides. Flow near the tips is the result of the combined action of vortex rings, concentration shells, and rolls.

While electric and buoyancy forces are normal to each other in a horizontal cell, in vertical cells, cathode above anode, both forces are coplanar and have the same direction. This is, naturally, the fundamental cause of their different behavior.

Mathematical modeling is supported by 3D numerical simulation results shown in Figures 3.1 (horizontal cell), 3.3 (vertical cell, cathode above anode), and 3.5 (vertical cell, cathode below anode), respectively.

3D numerical simulations are validated by the corresponding 2D experimental measurements presented in Figures 1.3 and 1.4 for horizontal cells, and in Figures 1.6 and 1.7 for vertical cells, respectively.

In conclusion, the numerical simulation of our 3D mathematical model makes it possible to prove from first principles the existence of 3D structures, and therefore it leads to a more complete formulation of a 3D phenomenological model and its space-time evolution: rolls are vortex tubes squeezed at their ends, concentration fronts form shells accompanying rolls, electric spherical drops are isosurfaces of the modulus of the electric field, roll, and shell envelope filaments, among other features. Thus, the model not only correctly predicts 2D experimental measurements found in the literature, but it also provides new insights into the physical problem.

Acknowledgments. This work is partially supported by UBACYT Grant X132/2008, CONICET Grant PIP5756/06, and ANPCyT Grants PICTR 184/02 and PAV 127/03. We are grateful to G. González for providing Figures 1.5, 1.6, and 1.7.

REFERENCES

- [1] F. ARGOUL, J. HUTH, P. MERZEAU, A. ARNÉODO, AND H. L. SWINNEY, *Experimental evidence for homoclinic chaos in an electrochemical growth process*, Phys. D, 62 (1993), pp. 170–185.
- [2] A. J. BARD AND L. R. FAULKNER, *Electrochemical Methods: Fundamentals and Applications*, John Wiley & Sons, New York, 1980.
- [3] D. P. BARKEY, D. WATT, Z. LIU, AND S. RABER, *The role of induced convection in branched electrodeposit morphology selection*, J. Electrochem. Soc., 141 (1994), pp. 1206–1212.
- [4] R. M. BRADY AND R. C. BALL, *Fractal growth of copper electrodeposits*, Nature, 309 (1984), pp. 225–229.
- [5] J.-N. CHAZALVIEL, *Electrochemical aspects of the generation of ramified metallic electrodeposits*, Phys. Rev. A, 42 (1990), pp. 7355–7367.
- [6] J. R. DE BRUYN, *Fingering instability of gravity currents in thin-layer electrochemical deposition*, Phys. Rev. Lett., 74 (1995), pp. 4843–4846.
- [7] S. DENGRA, *Experimental and theoretical studies of ion transport in thin-layer electrodeposition cells*, Ph.D. thesis, Departamento de Computación, Universidad de Buenos Aires, Buenos Aires, 2004.
- [8] S. DENGRA, G. MARSHALL, AND F. MOLINA, *Front tracking in thin-layer electrodeposition*, J. Phys. Soc. Japan, 69 (2000), pp. 963–971.
- [9] V. FLEURY AND J.-N. CHAZALVIEL, *2-D and 3-D convection during electrochemical deposition, experiments and models*, in Fractal Aspects of Materials, F. Family, P. Meakin, B. Sapoval, and R. Wool, eds., vol. 367 of MRS Symposium Proceedings Series, Material Research Society, Warrendale, Pennsylvania, 1995, pp. 169–176.

- [10] V. FLEURY, J.-N. CHAZALVIEL, AND M. ROSSO, *Theory and experimental evidence of electroconvection around electrochemical deposits*, Phys. Rev. Lett., 68 (1992), pp. 2492–2495.
- [11] ———, *Coupling of drift, diffusion, and electroconvection, in the vicinity of growing electrodeposits*, Phys. Rev. E, 48 (1993), pp. 1279–1295.
- [12] V. FLEURY, J. KAUFMAN, AND B. HIBBERT, *Mechanism of a morphology transition in ramified electrochemical growth*, Nature, 367 (1994), pp. 435–438.
- [13] V. FLEURY, M. ROSSO, AND J.-N. CHAZALVIEL, *Recent progress in electrochemical deposition without supporting electrolyte*, in Fractal Aspects of Materials, F. Family, P. Meakin, B. Sapoval, and R. Wool, eds., vol. 367 of MRS Symposium Proceedings Series, Material Research Society, Warrendale, Pennsylvania, 1995, pp. 183–194.
- [14] ———, *Diffusion migration and convection in electrochemical deposition, vortex pairs, vortex ring arches and domes*, in Defect Structure, Morphology, and Properties of Deposits, H. D. Merchant, ed., TMS Publications, Warrendale, Pennsylvania, 1995, pp. 195–217.
- [15] V. FLEURY, M. ROSSO, J.-N. CHAZALVIEL, AND B. SAPOVAL, *Experimental aspects of dense morphology in copper electrodeposition*, Phys. Rev. A, 44 (1991), pp. 6693–6705.
- [16] G. GONZÁLEZ, G. MARSHALL, F. MOLINA, AND S. DENGRA, *Transition from gravito- to electroconvective regimes in thin-layer electrodeposition*, Phys. Rev. E, 65 (2002), 051607 (8 pages).
- [17] G. GONZÁLEZ, G. MARSHALL, F. V. MOLINA, S. DENGRA, AND M. ROSSO, *Viscosity effects in thin-layer electrodeposition*, J. Electrochem. Soc., 148 (2001), pp. C479–C487.
- [18] J. HUTH, H. SWINNEY, W. MCCORMICK, A. KUHN, AND F. ARGOUL, *Role of convection in thin-layer electrodeposition*, Phys. Rev. E, 51 (1995), pp. 3444–3458.
- [19] C. LÉGER, J. ELEZGARAY, AND F. ARGOUL, *Experimental demonstration of diffusion-limited dynamics in electrodeposition*, Phys. Rev. Lett., 78 (1997), pp. 5010–5013.
- [20] V. G. LEVICH, *Physicochemical Hydrodynamics*, Prentice Hall, Englewood Cliffs, New Jersey, 1962.
- [21] K. A. LINEHAN AND J. R. DE BRUYN, *Gravity currents and the electrolyte concentration field in electrochemical deposition*, Canad. J. Phys., 73 (1995), pp. 177–186.
- [22] G. D. MALLINSON AND G. DE VAHL DAVIS, *Three-dimensional natural convection in a box: A numerical study*, J. Fluid Mech., 83 (1977), pp. 1–31.
- [23] G. MARSHALL, E. MOCOSKOS, F. V. MOLINA, AND S. DENGRA, *Three-dimensional nature of ion transport in thin-layer electrodeposition*, Phys. Rev. E, 68 (2003), 021607 (8 pages).
- [24] G. MARSHALL AND P. MOCOSKOS, *Growth model for ramified electrochemical deposition in the presence of diffusion, migration, and electroconvection*, Phys. Rev. E, 55 (1997), pp. 549–563.
- [25] G. MARSHALL, P. MOCOSKOS, H. L. SWINNEY, AND J. M. HUTH, *Buoyancy and electrically driven convection models in thin-layer electrodeposition*, Phys. Rev. E, 59 (1999), pp. 2157–2167.
- [26] G. MARSHALL, F. V. MOLINA, AND A. SOBA, *Ion transport in thin cell electrodeposition: modelling three-ion electrolytes in dense branched morphology under constant voltage and current conditions*, Electrochimica Acta, 50 (2005), pp. 3436–3445.
- [27] G. MARSHALL, E. PERONE, P. TARELA, AND P. MOCOSKOS, *A macroscopic model for growth pattern formation of ramified copper electrodeposits*, Chaos Solitons Fractals, 6 (1995), pp. 315–324.
- [28] J. NEWMAN AND K. THOMAS-ALEA, *Electrochemical Systems*, 3rd ed., John Wiley & Sons, Hoboken, New Jersey, 2004.
- [29] *OpenDX: An open source imaging package*. Available at <http://www.opendx.org>.
- [30] K. PIETRONERO AND H. J. WEISMANN, *Stochastic model for dielectric breakdown*, J. Statist. Phys., 36 (1984), pp. 909–916.
- [31] R. F. PROBSTEIN, *Physicochemical Hydrodynamics: An Introduction*, 2nd ed., John Wiley & Sons, New York, 1994.
- [32] T. VICSEK, *Fractal Growth Phenomena*, 2nd ed., World Scientific, Singapore, 1992.